MoS_2 Field-Effect Transistor for Next-Generation Label-Free Biosensors

Deblina Sarkar,[†,*] Wei Liu,[†] Xuejun Xie,[†] Aaron C. Anselmo,[‡] Samir Mitragotri,[‡] and Kaustav Banerjee[†,*]

[†]Department of Electrical and Computer Engineering and [‡]Department of Chemical Engineering, University of California, Santa Barbara, California 93106, United States

ABSTRACT

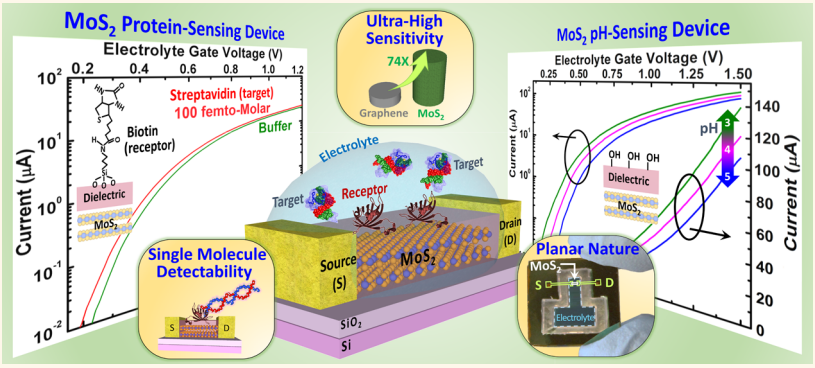

Biosensors based on field-effect transistors (FETs) have attracted much attention, as they offer rapid, inexpensive, and label-free detection. While the low sensitivity of FET biosensors based on bulk 3D structures has been overcome by using 1D structures (nanotubes/nanowires), the latter face severe fabrication challenges, impairing their practical applications. In this paper, we introduce and demonstrate FET biosensors based on molybdenum disulfide (MoS_2), which provides extremely high sensitivity and at the same time offers easy patternability and device fabrication, due to its 2D atomically layered structure. A MoS_2-based pH sensor achieving sensitivity as high as 713 for a pH change by 1 unit along with efficient operation over a wide pH range (3—9) is demonstrated. Ultrasensitive and specific protein sensing is also achieved with a sensitivity of 196 even at 100 femtomolar concentration. While graphene is also a 2D material, we show here that it cannot compete with a MoS_2-based FET biosensor, which surpasses the sensitivity of that based on graphene by more than 74-fold. Moreover, we establish through theoretical analysis that MoS_2 is greatly advantageous for biosensor device scaling without compromising its sensitivity, which is beneficial for single molecular detection. Furthermore, MoS_2, with its highly flexible and transparent nature, can offer new opportunities in advanced diagnostics and medical prostheses. This unique fusion of desirable properties makes MoS_2 a highly potential candidate for next-generation low-cost biosensors.

KEYWORDS: 2D materials · MoS_2 · biosensor · dichalcogenides · field-effect transistor · label-free · pH sensor

Biosensors are of paramount importance not only in the field of medical diagnostics but also for national security, forensic industries, and environmental monitoring. Especially, interest in biosensors based on field-effect transistors (FETs)[1] is fomented by their highly desirable attributes such as rapid electrical detection without the need for labeling the biomolecules, low power consumption, portability, inexpensive mass production, and the possibility of on-chip integration of both sensor and measurement systems. In a conventional FET used for digital applications, two electrodes (source and drain) are used to connect a semiconductor material (channel). Current flowing through the channel between the source and drain is electrostatically modulated by a third electrode called the gate, which is capacitively coupled through a dielectric layer covering the channel region. In the case of an FET biosensor (Figure 1a), the physical gate present in a logic transistor is removed and the dielectric layer is functionalized with specific receptors for selectively capturing the desired target biomolecules. The charged biomolecules when captured produce a *gating* (electrostatic) *effect*, which is transduced into a readable signal in the form of change in electrical characteristics of the FET such as drain-to-source current or channel conductance. It is to be noted here that apart from the dielectric layer, different polymers/lipids

* Address correspondence to deblina@ece.ucsb.edu, kaustav@ece.ucsb.edu.

Received for review February 14, 2014 and accepted March 3, 2014.

Published online March 03, 2014
10.1021/nn5009148

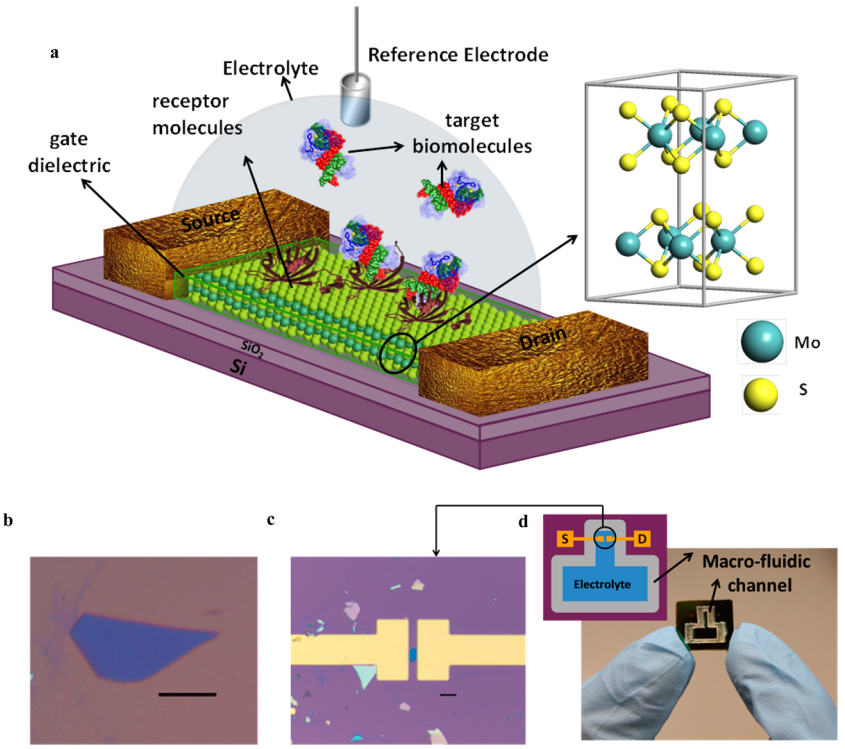

Figure 1. MoS_2-based FET biosensor device. (a) Schematic diagram of MoS_2-based FET biosensor. For biosensing, the dielectric layer covering the MoS_2 channel is functionalized with receptors for specifically capturing the target biomolecules. The charged biomolecules after being captured induce a gating effect, modulating the device current. An electrolyte gate in the form of a Ag/AgCl reference electrode is used for applying bias to the electrolyte. The source and drain contacts are also covered with a dielectric layer to protect them from the electrolyte (not shown in this figure). (b) Optical image of a MoS_2 flake on 270 nm SiO_2 grown on degenerately doped Si substrate. Scale bar, 10 μm. (c) Optical image of the MoS_2 FET biosensor device showing the extended electrodes made of Ti/Au. Scale bar, 10 μm. (d) Image and schematic diagram (inset figure) of the chip with the biosensor device and macrofluidic channel for containing the electrolyte. Inlet and outlet pipe for transferring the fluid and the reference electrode are not shown in the figure.

have also been used to cover the channel, and in several cases direct functionalization of the channel using specific groups/linkers/receptors has been done (Supporting Information S1). However, as long as an unambiguous transduction mechanism through an electrostatic effect is achieved (now the effect can take place through any layer (we call it the *effective layer*), be it dielectric, lipid, polymer, linker/receptor layers, or any other groups), the general conclusions presented in this work remain valid.

Given the importance of FET biosensors, there has been a lot of work on identifying an appropriate channel material for the same. Among the various materials reported, nanostructured carbon nanotubes (CNTs) and Si nanowires (NWs) have been found to be most attractive due to their size compatibility and ability to provide high sensitivity.[2,3] However, the same 1D nature that leads to efficient electrostatics and hence higher sensitivity also leads to difficulty in fabrication, thereby creating a major challenge for the success of 1D technologies. While the top-down fabrication technique for 1D structures suffers from high cost and slow production rate,[4] the bottom-up method faces severe integrability issues,[2,4] thus hampering the practical usability of such structures. The 2D materials, on the other hand, are highly promising, as they not only can provide excellent electrostatics due to their atomically thin structures but also possess planar nature, which is amenable to large-scale integrated device processing and fabrication. It is worth noting that thinning down of 3D materials, such as Si, into 2D structures not only is fabrication-wise expensive but would also suffer severely due to interface defects and uncontrollable band-gap variation when scaled down. Hence, naturally 2D layered materials are desirable, leading to interest in graphene[5] based FET biosensors.[2,6−9] However, we show here that the lack of a band gap in graphene fundamentally limits its sensitivity. In this Article, we bring forward the tremendous potential of MoS_2,[10−17] which is a biocompatible material,[18] as the channel material in label-free FET biosensors. MoS_2 belongs to the class of transition-metal dichalcogenides (TMDs),[10−14,19−22] which consist of 2D stacked layers of covalently bonded transition metal and dichalcogenide atoms arranged in a hexagonal lattice where adjacent layers are held together by relatively weak van der Waals forces. Due to this weak interlayer bonding in TMDs, it is possible to obtain atomically thin films with pristine interfaces, a monolayer of MoS_2 being only around 0.65 nm thick.

While MoS_2-based photodetectors,[23] fluorogenic nanoprobes,[24] gas detectors,[25−28] chemical sensors,[29] and electrodes for electrochemical sensing[30] have been reported in the literature, this work represents the first demonstration of MoS_2 (for that matter any TMD)-based FET biosensors working in an aqueous environment and in subthreshold region, which is capable of ultrasensitive and specific detection of biomolecules.[31] We demonstrate that the proposed biosensor achieves excellent sensitivity for pH sensing as well as biomolecule detection. Also, MoS_2 has pristine surfaces (without out-of-plane dangling bonds), which reduces surface roughness scattering and interface traps. This results in a low density of interface states on the semiconductor-dielectric interface, which can lead to not only better electrostatic control but also reduction in low-frequency (flicker) noise, which is one of the main sources of noise in FET biosensors.[32] In addition, we show through rigorous theoretical calculations that MoS_2-based biosensors can achieve ultimate scaling limits while retaining high sensitivity, which is useful for detection at low biomolecular concentrations as well as reduction in power and space requirements, crucial for achieving dense integrated structures. Furthermore, ultrathin MoS_2 possesses transparency[33] as well as high flexibility and mechanical strength.[13] MoS_2 devices fabricated on transparent and flexible substrates can adapt to the curvilinear surfaces of the human body and thereby hold great promise for wearable and implantable biosensor devices. The recent developments in liquid-scale exfoliation[34,35] and chemical vapor deposition growth[36,37] as well as demonstration of fully integrated multistage logic circuits on MoS_2[38] indicate feasibility for large-scale and low-cost processing of highly integrated and multiplexed MoS_2 FET-based sensor architectures.

RESULTS AND DISCUSSION

Biosensor Characterization. The micromechanical exfoliation technique, which has been widely employed for prototyping experiments on various 2D materials,[7,10−14,19−22] has been used to obtain the MoS_2 flakes (Figure 1b). However, large-area synthesis of MoS_2 has already been achieved as mentioned above,[34−37] which indicates that the proposed biosensor device fabrication can be scaled up in the near future. The devices (Figure 1c) were fabricated on 270 nm SiO_2/Si substrates with 60 nm/100 nm Ti/Au as source and drain metal contacts and 30−35 nm of high-k dielectric hafnium oxide (HfO_2) as gate dielectric (details of device characterization presented in Supporting Information S2). It has been shown in previous works that if the source/drain metal electrodes are not passivated and thus are in direct contact with the electrolyte, the biomolecules can get adsorbed directly on the electrodes, changing the local work function of the metal and hence the contact resistance.[39,40] To avoid this issue in this work, the source and drain contacts are passivated with a dielectric layer to protect them from the electrolyte. A fluidic channel (Figure 1d) for containing the electrolyte is fabricated using an acrylic sheet. An Ag/AgCl reference electrode, referred to as the electrolyte gate, is used to apply bias to the electrolyte, which is necessary for the stable operation as well as for controlling the operation regime of the biosensor.[41] First the electrical characterization of the devices is carried out in a dry environment by measuring the transfer characteristics as a function of drain and back gate voltages (the highly doped Si and the 270 nm SiO_2 act as the back gate and the gate dielectric, respectively), illustrating n-type FET characteristics (Figure 2a and b). High back gate voltage is required to turn on the device due to the presence of very thick back gate oxide. For biosensing applications, it is necessary that the devices are able to operate in a wet environment. Hence, the devices were measured in a wet environment by transferring electrolyte solution (0.01 × Phosphate Buffered Saline (PBS)) to the fluidic channel. Figure 2c and d illustrates that efficient control of the proposed biosensor device is possible in the wet environment with the successful demonstration of electrolytic top gating on the MoS_2 channel.

pH Sensing. The operation of a MoS_2 biosensor is first demonstrated for the case of detection of pH changes of the electrolytic solution. The pH sensing is based on the protonation/deprotonation of the OH groups on the gate dielectric (Figure 3a) depending on the pH value of the electrolyte, thereby changing the dielectric surface charge. A solution with lower pH value would tend to protonate ($OH + H^+ = OH_2^+$) the surface OH groups, thereby generating positive surface charges on the dielectric while that with higher pH value would tend to deprotonate ($OH - H^+ = O^-$) the surface OH groups generating negative charges. This pH-dependent surface charge together with the electrolyte gate voltage applied through the reference electrode determines the effective surface potential of the dielectric. The drain current as a function of the electrolyte gate voltage for different pH values of the electrolyte is shown in Figure 3b. A significant increase in current is obtained at a particular applied bias with decrease in pH value (or higher positive charge on the dielectric surface that causes lowering of the threshold voltage of the FET), leading to the successful demonstration of the MoS_2 pH sensor. The shift in threshold voltage (which has been calculated using the extrapolation in the saturation region (ESR) method[42]) is found to be 59 mV/pH. This threshold voltage shift can be understood from the following discussion. The change in surface charge on a dielectric with a change in pH of the electrolyte can be found by considering the protonation/deprotonation reactions with their respective dissociation constants and the number of sites on the dielectric per unit area (which can be either

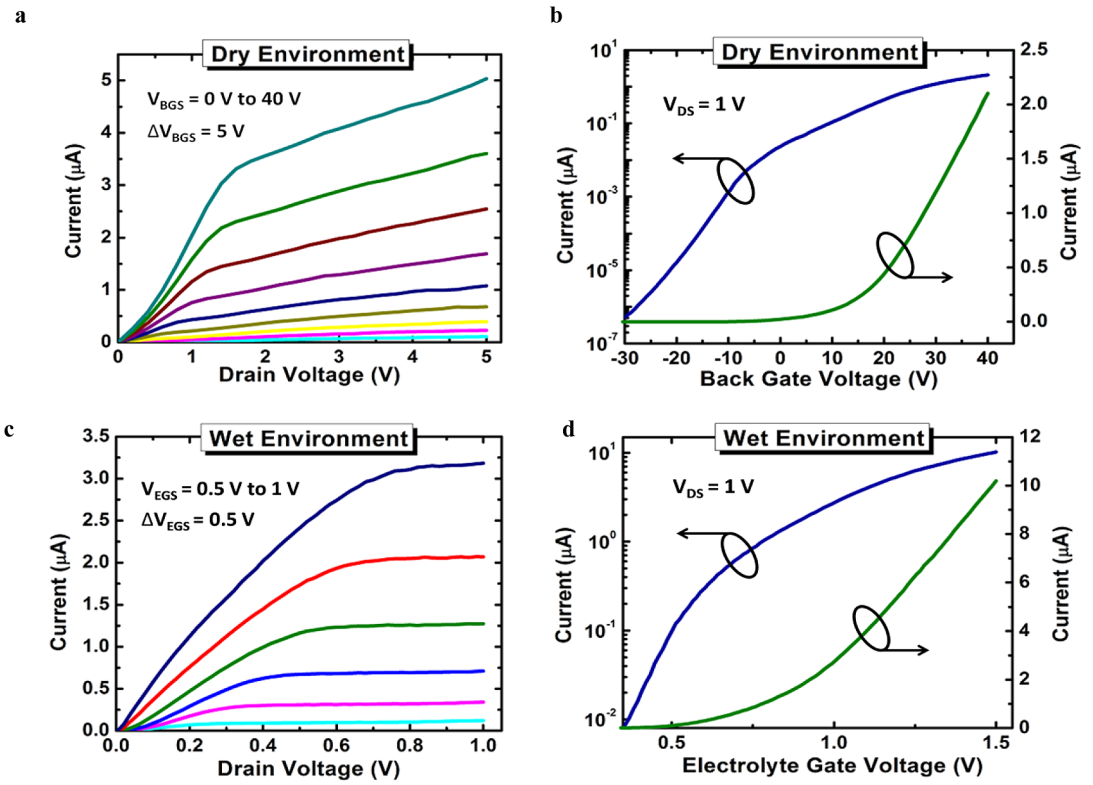

Figure 2. Electrical characterization of a MoS_2 FET sensor in dry and wet environment. (a) Drain current as a function of drain voltage with the back gate voltage (V_{BGS}) varying from 0 to 40 V in steps of 5 V. The thickness of the MoS_2 used is 5 nm. (b) Drain current *versus* back gate voltage with drain voltage fixed at 1 V. Left axis shows current in logarithmic scale, while right axis shows that in linear scale. (c) Drain current as a function of drain voltage with the back gate voltage floating and electrolyte gate voltage (V_{EGS}) varying from 0.5 to 1 V in steps of 0.5 V with observation of robust current saturation. The electrolyte used is 0.01× PBS solution. (d) Drain current *versus* electrolyte gate voltage with drain voltage fixed at 1 V.

protonated, deprotonated, or neutral). The change in surface potential can be found by relating it to this charge through the electrical surface capacitance and can be written as[43]

$$\frac{d\phi_s}{dpH} = -2.3\alpha\frac{k_B T}{q} \quad (1)$$

$$\alpha = \left(2.3\frac{k_B T}{q^2}\frac{C_S}{\beta_S}+1\right)^{-1} \quad (2)$$

where ϕ_s is the surface potential on the gate dielectric, k_B is the Boltzmann constant, T is temperature, q is electronic charge, C_S is electrical surface capacitance, and β_S is intrinsic buffer capacity, which represents the change in the surface charge with the change in pH of the solution near the surface. The ideal change in surface potential that can be obtained is 59.6 mV/pH at 300 K when α approaches 1. When the intrinsic buffer capacity of the dielectric surface is high, α can reduce to 1, leading to almost ideal response, which has been shown to be the case for HfO_2.[44] This has also been confirmed by our investigations.

Sensitivity for pH sensing (defined as $S_{n\_pH} = (I_{pH2} - I_{pH1})/I_{pH1} \times 100$, where I_{pH1} and I_{pH2} are the values of transistor current at two different pH's of the electrolyte, pH1 and pH2, respectively, where pH1 > pH2) is deduced from the curves in subthreshold, saturation, and linear regions. Figure 3c shows the comparison of pH sensitivity in these three different regions. In the subthreshold region, the drain current has exponential dependence on the gate dielectric surface potential, while in saturation and linear regions the relationship is quadratic and linear, respectively. Hence the sensitivity in the subthreshold region is much higher compared to those in the saturation and linear regions.[41,45] Sensitivity values as high as 697 and 713 are obtained for pH changes from 3 to 4 and 4 to 5, respectively. The critical parameter of an FET, which gives an indication of the efficiency of gating effect and hence the sensitivity of the biosensor, is the subthreshold swing (SS).[41] SS is defined as the inverse of the slope of their $\log_{10}(I_D)-V_{GS}$ curve, where I_D and V_{GS} are the drain-to-source current and gate-to-source voltage, respectively. Therefore, the SS of a device essentially indicates the change in gate voltage required to change the subthreshold current by one decade ($SS = dV_{GS}/d(\log_{10}(I_D))$). Thus, the smaller the SS, the higher the change in current for a particular change in the dielectric surface potential due to gating effect produced by the pH change or attachment of biomolecules and hence the higher the sensitivity (details in Supporting Information S3). The ultrathin nature of the MoS_2 and

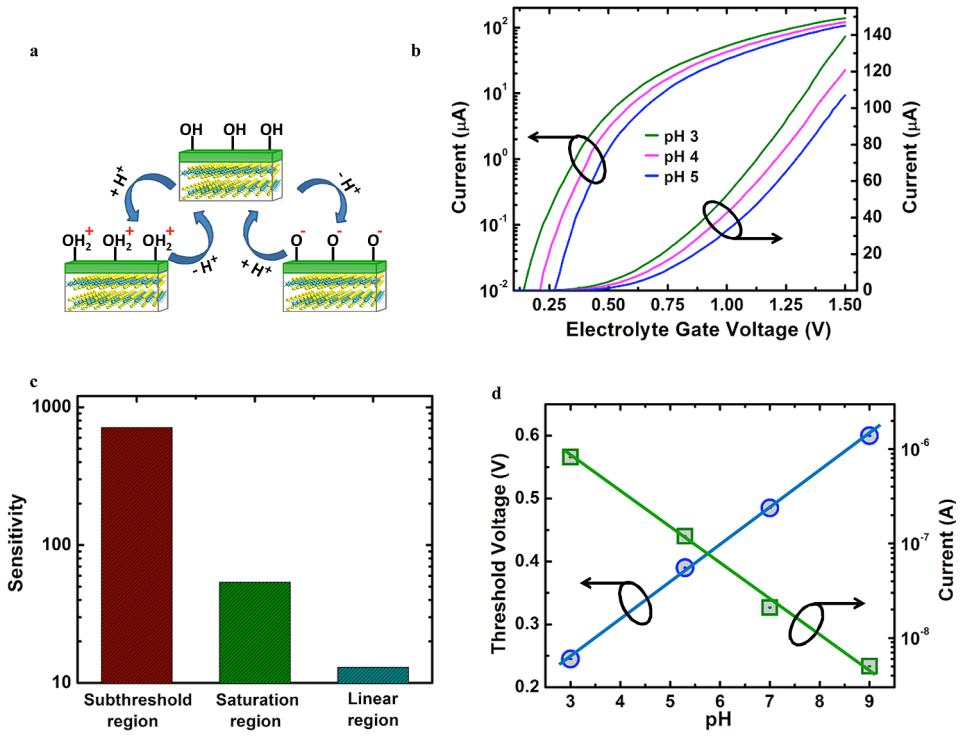

Figure 3. MoS_2 FET sensor for pH sensing. (a) Illustration of the principle of pH sensing. At lower pH (higher concentration of H^+ ions), the OH group on the dielectric surface gets protonated to form OH_2^+, leading to a positive surface charge on the dielectric, while at higher pH, the OH group gets deprotonated to form O^-, leading to a negative surface charge on the dielectric. (b) Drain current for an n-type MoS_2 FET-based pH sensor is plotted as a function of electrolyte gate voltage for three different pH values of the solution. The thickness of the MoS_2 used is around 2 nm, and the SS obtained is around 78 mV/decade. A decrease in pH values leads to an increase in device current, consistent with higher positive charge at lower pH and n-type behavior of the FET biosensor. (c) Comparison of sensitivity in subthreshold, saturation, and linear region for a pH change of 4 to 5 of the electrolyte solution derived from the I_d-V_g curves shown in (b). The subthreshold region shows a substantially higher sensitivity of 713, while the saturation and linear regions exhibit much lower sensitivities of 53.69 and 12.96, respectively. (d) Change in threshold voltage and current of the MoS_2 FET for a wide range of pH (3−9). Left axis shows the threshold voltages, while right axis corresponds to the current in the subthreshold region. The thickness of the MoS_2 used is around 15 nm. The subthreshold swing of the device was found to be around 208 mV/decade.

its pristine interfaces lead to excellent SS and hence high sensitivity of the proposed device in spite of the presence of a very thick gate dielectric (30 nm). In Figure 3d we show the current as well as the threshold voltages for a large pH range (3−9) (I_d-V_g curves shown in Supporting Information S4). From our measurements, the shift in threshold voltage (59 mV/pH) is linear over the wide pH range (3−9).

Specific Detection of Biomolecules. Next, the specific sensing of biomolecules using the MoS_2 biosensor is investigated through the well-known biotin−streptavidin interaction where the biotin and streptavidin act as models for receptor and target molecules, respectively. Figure 4a shows that a device functionalized with biotin exhibited a substantial decrease in current on addition of streptavidin solution (10μM in 0.01 × PBS) compared to that measured in pure buffer (0.01 × PBS) without streptavidin. This is in agreement with the negative charge of the streptavidin, as the pH of 0.01 × PBS is greater than the *isoelectric point* (abbreviated as pI and defined for a particular molecule as the pH at which that molecule is neutral) of streptavidin. Addition of pure buffer again caused a negligible change in current consistent with the strong binding between biotin and streptavidin. To rule out the possibility of nonspecific interactions and false signals, a number of control experiments are carried out. First, an unfunctionalized device exhibited similar current levels in pure buffer and streptavidin solution (Figure 4b), indicating the absence of false signals. Second, a lower value of pH (<pI of streptavidin and thereby attributing a positive charge to it) was used, and it is observed that the addition of streptavidin solution to a device functionalized with biotin leads to an increase in current compared to that in pure buffer (Figure 4c). In yet another experiment, a device functionalized with biotin did not result in current change (Figure 4d) on addition of immunoglobulin G (IgG), which is not specific for biotin, confirming the absence of nonspecific bindings. All these experiments were done with comparatively thicker MoS_2 flakes, which are relatively easier to locate optically on the substrate. In order to obtain improved SS and, hence, sensitivity, ultra-thin-layer MoS_2 consisting of only four atomic layers was explored (Figure 4e and f). An excellent SS of 90 mV/dec was obtained even with a very thick dielectric layer

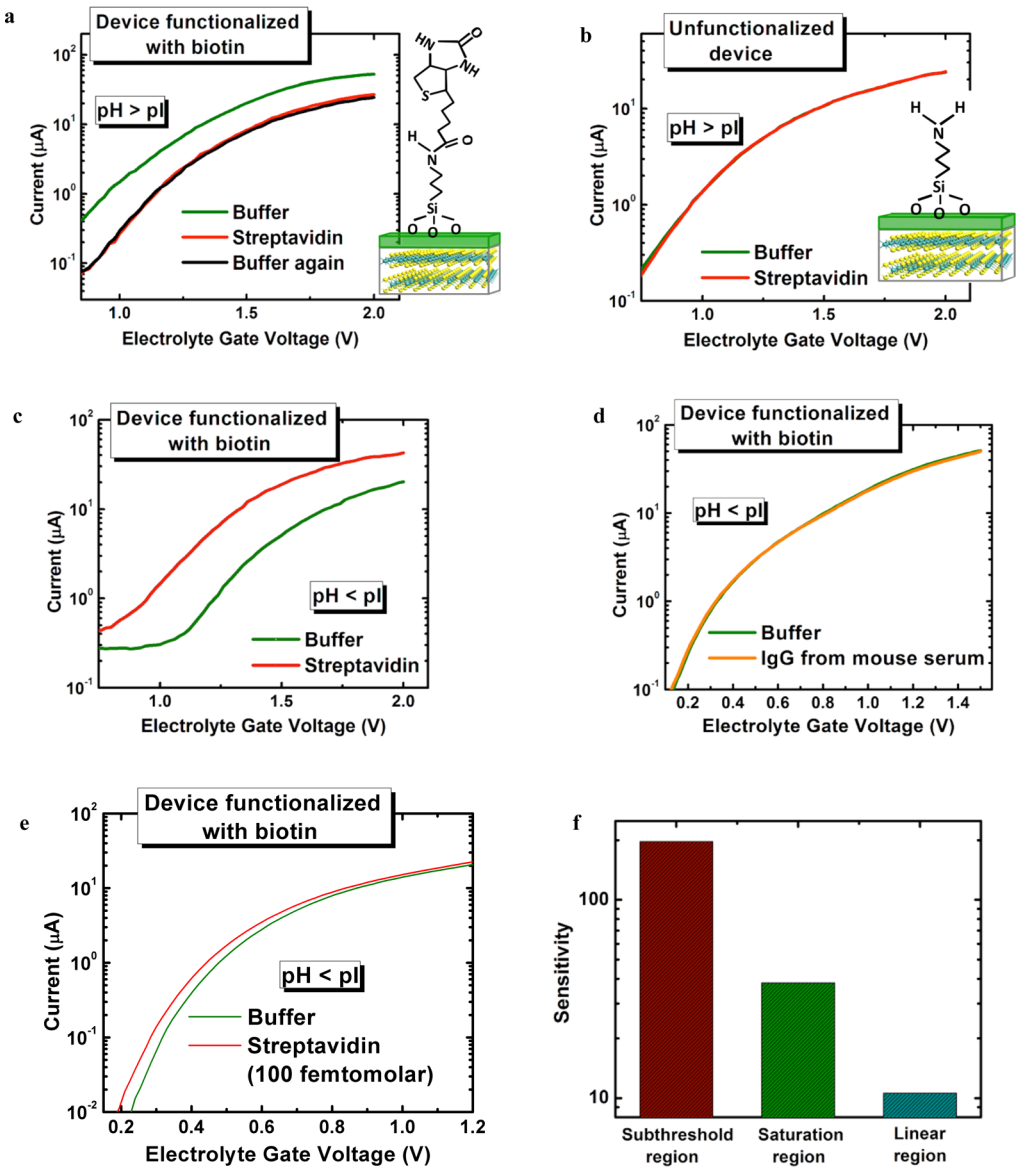

Figure 4. MoS_2 FET sensor for specific detection of biomolecules. (a) A device functionalized with biotin (as shown by the schematic diagram) was first measured in pure buffer (0.01× PBS), as shown by the green curve. Addition of streptavidin solution (10 μM in 0.01× PBS) leads to decrease in current (red curve) due to the negative charge of the protein, as the pH of the solution is more than the pI of streptavidin. The device is then measured again in pure buffer, leading to no significant change (black curve). (b) An unfunctionalized device (device with only 3-aminopropyl(triethoxy)silane (APTES) attached to it but not functionalized with biotin), as shown by the schematic diagram, exhibits similar current in pure buffer and streptavidin solution (solutions used are the same as in (a)), confirming that there are no false signals. (c) Addition of streptavidin solution (10 μM) at a pH of 4.75, which is less than the pI of streptavidin, leads to an increase in current, consistent with the positive charge of the protein. (d) Addition of IgG (56 μg/mL) at pH of 4.75 (which is smaller than the pI of IgG) leads to a negligible change in the device current as IgG is not specific for biotin. (e) The high sensitivity of the MoS_2 biosensor device is illustrated for four-layer MoS_2 (around 2.7 nm thick), as a significant increase in current is obtained on addition of streptavidin solution (100 fM) at pH 3. (f) Comparison of sensitivities in the subthreshold, saturation, and linear regions showing that the subthreshold region has substantially higher sensitivity.

(35 nm). Sensitivity (defined as the ratio of the difference in current before and after biomolecule binding to the lower of the two currents) as high as 196 was achieved in the subthreshold region for a streptavidin solution of 100 fM. Similar to the case for pH sensing, sensitivity in the subthreshold region is significantly higher compared to those in the saturation and linear regions (Figure 4f). Note that, while in this work, we demonstrated the specific detection of biomolecules using streptavidin and biotin as examples of target and receptor molecules, respectively, the proposed biosensor can be used for selective sensing of other biomolecules as well. For this purpose, functionalization of the gate dielectric surface with respective specific receptors can be realized taking advantage of the vast body of literature that exists on the functionalization of oxides as well as semiconducting surfaces.[46−48] Also, in our experiments we have used biomolecules in

PBS solution, which is a standard procedure used for demonstrating the operation of FET-based biosensors.[2,3,7,45,49] It is to be noted that detection of biomolecules from whole blood using FET biosensors has already been demonstrated using a microfluidic purification chip.[50] This technique is independent of channel material and can also be extended to the MoS_2-based FET biosensor for detection of biomolecules in the complex environment of whole blood.

Scalability and Single-Molecule Detection Analysis. It is of particular interest in biosensing to detect biomolecules at very low concentrations; especially a biosensor that can detect down to a single molecule is highly desirable. Low concentration detection (LCD) is dependent on various factors including the site density on the effective layer, type of biomolecule, sensor area, analyte mass transport in the solution *etc.* Since in this paper, we are focusing on the channel material, we discuss the ways in which the channel material will impact the LCD. The channel material will be evaluated in terms of LCD through the criteria whether a few or in the most desired case a single biomolecule attached to the effective layer can cause measurable change in the current. In the case of graphene it has been shown that single gas molecules can be detected.[51] However, in this case the gas molecules dope the graphene by getting directly absorbed into it, which as discussed earlier leads to nonspecificity and is not desirable for biosensors. To achieve specificity, an effective layer is necessary (Supporting Information S1), and the fundamental limitations of graphene for electrostatic modulation of current through an effective layer are discussed in the next section. Single biomolecule detection has been reported using CNTs where the transduction mechanisms involve bridging a gap in the channel[52] or modulation of scattering[53] and not the electrostatic field effect. The limitations of CNTs for practical usability have been discussed earlier, and in addition creating bandgaps in CNTs requires complex processing and leads to low yield,[52] which negate the advantages of using a FET platform. Detection of a single virus with a Si NW FET[54] and a single bacterium using graphene[55] have been demonstrated. Viruses (around 100 nm) and bacteria (several micrometers) are typically of larger size. For detection of a single entity of smaller biomolecules such as DNA or small proteins (<10 nm) with high sensitivity using a FET biosensor, aggressive downscaling of device dimensions is required, as shown through theoretical analysis presented in Supporting Information S5. Scaling down the device length to a dimension similar to that in which charge due to biomolecule effects (we call it the *impact dimension*) can maximize the gating effect due to the charged biomolecule. However, it is shown in Supporting Information S5 that decreasing the channel length in a typical FET biosensor leads to an increase in sensitivity but only to a certain extent. Further downscaling beyond a certain length (which is still greater than the impact dimension) results in severe sensitivity degradation. This is due to the encroachment of the source/drain electric field into the channel at shorter channel lengths, which effectively lowers the influence of the biomolecule (gate) induced vertical electric field in the channel region. In order to recover the gain in sensitivity with length scaling, the channel thickness should be reduced simultaneously. As calculated in Supporting Information S5, detection of a single biomolecule having an impact dimension of 5 nm with high sensitivity demands a channel thickness of only a few atomic layers or a wrapped gate nanowire architecture with a radius of around 2 nm. While this stringent requirement necessitates complex growth and processing techniques for conventional semiconducting materials (Si, Ge, GaAs, *etc.*) with diamond/zinc-blende structure, it is easily satisfied by MoS_2 due to its atomically layered structure and pristine surfaces. Currently, the TMD technology is at an early phase and still undergoing development. Scaling down of the gate dielectric thickness remains to be achieved, and the dielectric thickness used in this paper is around 35 nm. In order to realistically determine the true potential of MoS_2 for single-molecule detection, such that its performance is not screened by the thick dielectric layer, rigorous quantum mechanical simulations based on a nonequilibrium Green's function formalism (Supporting Information S6) are performed to obtain the local density of states[56] as a function of applied biases (Figure 5a) and hence the current (Figure 5b). Thereby, it is shown that even at 5 nm channel length, MoS_2 can maintain excellent gate control over the channel, leading to near ideal SS (Figure 5b), which is critical for obtaining high sensitivity. Thus, MoS_2 is highly advantageous for scaling down of FET biosensor devices, which not only can lead to higher sensitivity for detection of single quanta of a biomolecular element especially when the entity is of smaller size (sub-10 nm) but can also highly facilitate low-power (due to lower OFF currents at low FET supply voltages) and high-density biosensor device architectures. The increase in response time associated with the analyte transport at low concentration (not associated with the channel material) could be addressed by methods for increasing total flux toward the sensor, for example, through application of electrostatic or magnetic fields.[57,58]

Comparison with Graphene. In previous sections, we discussed the superiority of MoS_2 with a 2D layered structure for FET-based biosensing compared to other conventional materials or 1D structures. It might be expected that graphene, which is also a 2D layered material, will share the same virtues as MoS_2. However, as discussed below, graphene suffers from fundamental constraints in sensitivity as well as detection limits (details in Supporting Information S7). In FETs where

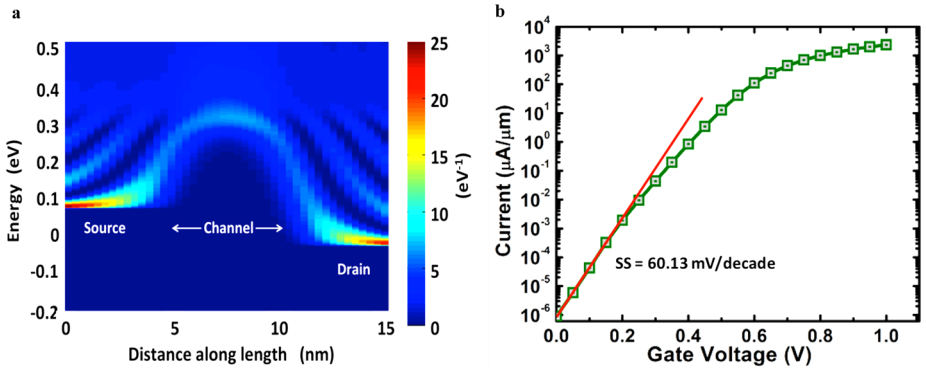

Figure 5. Ultrascaled MoS_2 device. Numerical results of rigorous quantum mechanical simulations based on nonequilibrium Green's function formalism. (a) Local density of states (LDOS) diagram as a function of energy (*y*-axis) and distance along the device length (*x*-axis) of a four-layer MoS_2 device with 5 nm channel length, 3 nm HfO_2 as gate dielectric, at a drain voltage of 0.1 V and gate voltage of 0.4 V. The density of states (in eV^{-1}) are local in the sense that they vary with position. The structure of LDOS varies with applied biases and illustrates the band bending in the channel. (b) Drain-to-source current as a function of gate-to-source voltage. An almost perfect subthreshold swing of 60.13 mV/decade is obtained, indicating highly efficient gate control even for an ultra-scaled channel length (5 nm).

semiconducting materials with a band gap serve as a channel, only electrons having energy higher than the source-to-channel barrier can transport from source to drain, as illustrated in Figure 6a. Hence, with lowering of the barrier more electrons can flow to the drain (Figure 6b), and since electrons occupy the energy levels according to the Boltzmann distribution at the source, the SS obtained can be as low as 60 mV/dec at room temperature (details in Supporting Information S7). However, if the band gap of the semiconducting material is extremely small, the barrier is extremely thin and even electrons having energies lower than the barrier height begin to flow *via* direct tunneling, as illustrated in Figure 6c. This leads to an increase in off-state leakage current, as shown in Figure 6d, and hence in the degradation of SS, as clear from Figure 6e, even though the simulation parameters related to channel thickness and dielectric properties have been chosen to achieve almost perfect electrostatics, *i.e.*, near-ideal change of potential at the interface of the semiconductor and the gate dielectric with a change in gate voltage. (It is to be noted that in the case of low-band-gap materials the term SS is used to denote the mathematical factor $dV_{GS}/d(\log_{10}(I_D))$ and not the swing in subthreshold region since the threshold voltage is not well defined due to high leakage.) Thus, the zero band gap of graphene leads to very high SS even though excellent electrostatics can be achieved due to its ultrathin nature (details in Supporting Information S7) and, hence, leads to low sensitivity. For experimentally demonstrating this fact, we explored graphene and the MoS_2 FET device with similar channel thickness, channel length, and top dielectric thickness, measured under similar conditions for the model case of pH sensing. The experimental findings are in-line with the theoretical predictions, as the graphene biosensor exhibits an SS of more than 5000 mV/dec even though it has an ultrathin body (Figure 6f). MoS_2 on the other hand, due to its ultrathin nature and pristine interfaces, not only can achieve excellent electrostatics but at the same time due to its sizable band gap (the band gap of MoS_2 varies in the range of 1.8 eV (for a monolayer) to 1.2 eV (for bulk)) can also suppress direct source-to-drain tunneling leakage currents (Fig. 6c), which degrade the SS at band gaps below around 0.4 eV (Figure 6e). A combination of both these factors leads to excellent SS in the case of MoS_2. Even with a very thick (35 nm) dielectric, MoS_2 with a similar thickness to graphene provides an excellent SS of 150 mV/dec. Hence, graphene provides a much lower sensitivity of 2.6 compared to that (193) achieved by MoS_2 (Figure 6g) for the same change in pH of the electrolyte (from a pH of 3 to a pH of 4). A graphene-based pH sensor reported in the literature[7] has shown a sensitivity of about 12 for a pH change of 1.1. In ref 7 the electrolyte is directly in contact with the graphene channel (without any dielectric layer), in which case the sensing mechanism is complicated, and in addition, for detection of biomolecules there is the possibility of nonspecific interactions. Moreover, since we measured the MoS_2 and graphene devices with the same dielectric thickness and under similar conditions, our values provide a more appropriate comparison. It is to be noted that opening a band gap in graphene remains extremely challenging,[59−62] and although there are several works on reduced graphene oxide based FET biosensors, the uncontrollable band gap together with the low purity of rGO leads to very low sensitivity (Supporting Information S7). On the other hand, while the other popular form of carbon, CNTs, possesses a band gap, their application as biosensors is severely limited due to the challenges in integrability as well as the chirality issue.[2]

CONCLUSIONS

In summary, we have demonstrated a FET biosensor based on the novel material MoS_2, whose

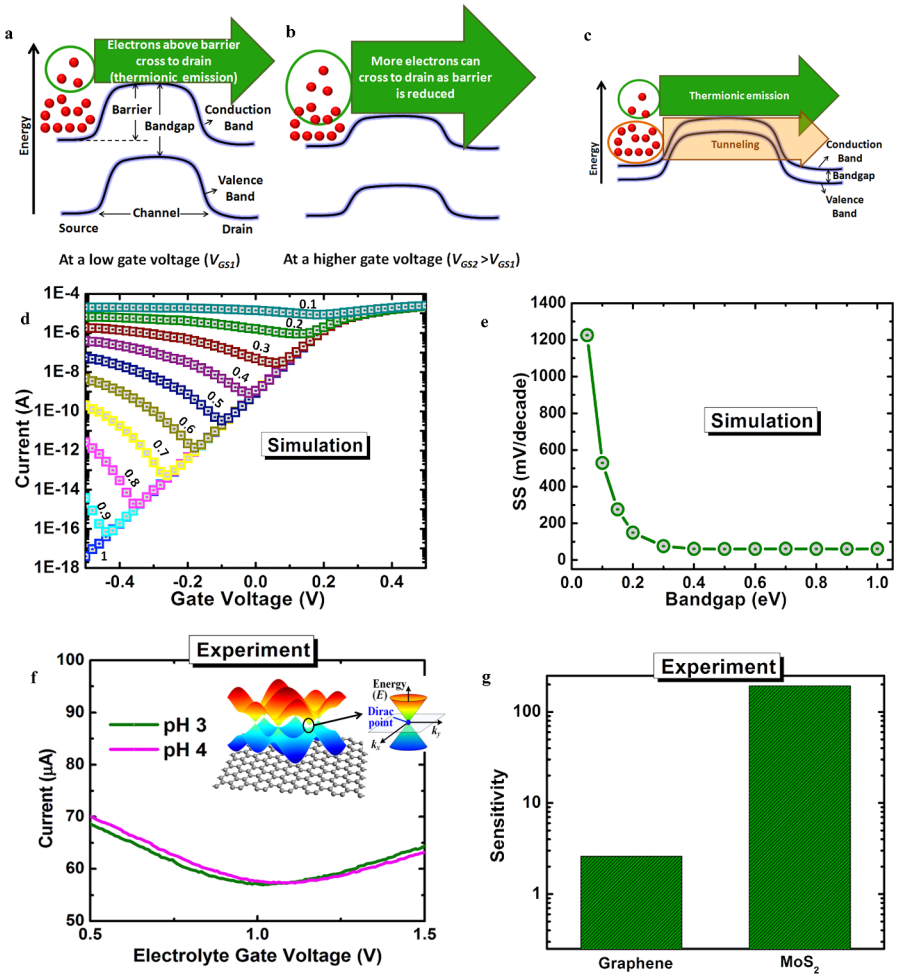

Figure 6. Band-gap effects and graphene FET biosensor. (a) Schematic band diagram illustrating the current flow mechanism in (n-type) FETs with the semiconducting layer having a considerable band gap. Only electrons having an energy greater than the barrier height can cross the barrier and contribute to current as shown by the green arrow. At low gate voltage (V_{GS1}), few electrons (within the green circle) can cross the barrier. (b) After the application of a higher gate voltage (V_{GS2}), more electrons (within the green circle) can cross the barrier. (c) In the case where the semiconducting channel has a very small band gap, not only can electrons flow above the top of the barrier, but electrons with lower energies can also tunnel through the barrier, which can increase the leakage current. (d) Current as a function of gate voltage for different band gaps of the semiconducting channel material varying from 1 to 0.1 eV. The corresponding band gap for each curve is shown in the figure. (e) Subthreshold swing as a function of band gap of the semiconducting channel material. (f) Graphene exhibits very little modulation of current and very high SS with variation of the electrolyte gate voltage. This is due to the lack of band gap in graphene, as illustrated through the band structure of graphene in the inset figure. A change in pH of the solution from 3 to 4 leads to significantly lower change in the current compared to that in the MoS_2-based pH sensor. The thickness of the graphene used in this experiment is around 7 nm. (g) Comparison of sensitivity of graphene and MoS_2-based FET biosensors for the same change in pH from 3 to 4. All device parameters in graphene and MoS_2 based FETs and the measurement conditions are kept identical for fair comparison. The sensitivity of the MoS_2-based FET biosensor is 74-fold higher compared to that based on graphene.

semiconducting nature together with the prowess of its 2D layered structure makes it highly advantageous for biosensing compared to other commonly used materials (Table 1). Not only can MoS_2 provide excellent electrostatics and sensitivity due to its atomically thin nature along with the presence of a band gap, it also provides a planar platform facilitating easy patternability, which together with the recent developments in large-scale MoS_2 production techniques can lead to fabrication of complex multiplexed sensor architectures with low cost, an imperative requirement for practical applications. A MoS_2-based pH sensor with ultrahigh sensitivity (713 for a pH change of 1 unit) as well as wide operation range (pH of 3 to 9) is demonstrated. Specific detection of protein is also demonstrated and an extremely high sensitivity of 196 was achieved even at 100 femtomolar concentration. Comparison of sensitivity in linear, saturation, and subthreshold regions is carried out for both pH and protein sensing, confirming the achievement of highest sensitivity in the subthreshold region. We also corroborated through theoretical and experimental study that graphene in spite of having a 2D nature and excellent electrostatics is fundamentally limited in sensitivity due to a lack of band gap. In addition, it is shown through theoretical analysis that MoS_2 can greatly

TABLE 1. Comparison of MoS_2 with Other Competing Materials for FET-Based Biosensing[a]

		sensitivity	device fabrication and large-scale integrability	device scalability	flexibility and transparency
3D bulk materials		*low (inferior electrostatic gating effect through biomolecule conjugation)*	possible	*low*	*low*
1D nanomaterials	Si NW	high (excellent electrostatic gating effect through biomolecule conjugation)	*(i) top-down method: high cost and slow production rate; (ii) bottom-up method: severe integrability issues*	possible but process-wise challenging	*low*
	CNT	high (excellent electrostatic gating effect through biomolecule conjugation)	*(i) separation of metallic and semiconducting nanotubes required; (ii) severe integrability issues*	possible but process-wise challenging	high
2D nanomaterials	graphene	*low (excellent electrostatic gating effect but low carrier modulation)*	(i) low-cost mass production possible; (ii) planar platform provides easy patternability and integrability	high	high
	MoS_2	high (excellent electrostatic gating effect through biomolecule conjugation)	(i) low-cost mass production possible; (ii) planar platform provides easy patternability and integrability	high	high

[a] Comparison is made in terms of factors that are specifically dependent on the channel material (and hence other factors that also influence biosensor performance but are not directly related to the channel material and are dependent on the properties of effective layers, biomolecules, or electrolyte are not included). Thus, apart from sensitivity, ease of the fabrication process (which determines whether a technology can be practically successful), device scalability (which is critical for detection of low concentrations of biomolecules as well as for reduction of power and space requirements), and flexibility and transparency (which is important for advanced diagnostics and implantable biosensors) have been included. It is clear that MoS_2 has the potential to overcome the material-dependent shortcomings (highlighted in italics) of previously reported materials.

facilitate device scalability, which can result in higher sensitivity for detection of single quanta of a biomolecule and can also lead to ultra-low-power and miniaturized biosensor devices, critical for hand-held diagnostic tools and point-of-care applications. Moreover, the highly flexible and transparent nature of MoS_2 is greatly advantageous for diagnostic purposes as well as artificial organ implantations. Since in this paper we have focused on bringing forward the potential of MoS_2 as a channel material for a FET biosensor, we discussed the factors that are affected specifically by the channel material. Other factors that can influence the biosensor performance such as properties of effective layers (including number of sites), biomolecules, and solution have been extensively reported and are not included, as they do not affect the fundamental conclusions of the paper with regard to evaluation of the channel material (Supporting Information S1). However, the proposed biosensor leverages the advantages of FET-based biosensing as mentioned earlier such as low response time, which is typical of FET biosensors in general and is dependent on analyte transport (and independent of the channel material). Moreover, excellent SS of the proposed biosensor may effectively help in rapid detection of low-concentration biomolecules (Supporting Information S8). Thus, this label-free, ultrasensitive, ultrascalable, and highly flexible sensor with low production cost and low power consumption can offer great opportunities in healthcare, security, and forensic industries and can provide better protection of our environment, food and water supplies.

METHODS/EXPERIMENTAL SECTION

The MoS_2 flakes were exfoliated on 270 nm SiO_2 grown through thermal oxidation of degenerately doped Si substrates. SiO_2 (270 nm) provides sufficient contrast for optical detection of MoS_2 flakes. The flakes were characterized using optical microscopy and atomic force microscopy (AFM) (Figure S1 in Supporting Information S2). For device fabrication, the source and drain regions were defined by photolithography followed by electron beam (e-beam) deposition of 60 nm/100 nm Ti/Au. The channel length defined by photolithography was 5 μm. Note that, in contrast to e-beam lithography generally used for making contacts to TMDs, we used photolithography to facilitate the fabrication of extended source/drain electrodes such that the source/drain contact pads are 2 mm away from the active region of the device in order to ensure that the measurement probes are kept away from the electrolyte. In order to fabricate biosensors with shorter channel lengths, a two-step lithography step can be adopted wherein the contact to the MoS_2 can be fabricated using e-beam lithography, while the extended electrodes can be fabricated using photolithography. After the source and drain formation, 30–35 nm of high-k dielectric hafnium oxide was deposited using atomic layer deposition at 200 °C. For specific detection of biomolecules, the dielectric surface was silanized using 3-aminoisopropyl(triethoxy)silane (APTES) obtained from Sigma Aldrich. Attachment of biotin was carried out using *N*-hydroxysulfosuccinimide (sulfo-NHS)-biotin obtained from Pierce Biotechnology. A macrofluidic channel for containing

the electrolyte was fabricated using an acrylic sheet. This macrochannel leads to a simple arrangement, as well as avoids diffusion-related limitations of microchannels.[49]

Conflict of Interest: The authors declare no competing financial interest.

Supporting Information Available: The Supporting Information includes the details on the transduction mechanism and sensor performance, MoS_2-based FET biosensor device characterization, dependence of sensitivity on subthreshold swing, additional data for the pH sensor, theoretical analysis of sensitivity for small-molecule detection, details of nonequilibrium Green's function formalism, additional details on dependence of biosensor performance on band gap and comparison with graphene, effect of subthreshold swing on response time and advantage of MoS_2. This material is available free of charge *via* the Internet at http://pubs.acs.org.

Acknowledgment. This work was supported in part by the National Science Foundation under Grant CCF-1162633. All process steps for device fabrication were carried out using the Nanostructure Cleanroom Facility at the California NanoSystems Institute and the Nanofabrication Facilities at UCSB, part of the National Nanotechnology Infrastructure Network. The authors made extensive use of the MRL Central Facilities at UCSB, which are supported by the MRSEC Program of the NSF (under Award No. DMR 1121053), a member of the NSF-funded Materials Research Facilities Network (www.mrfn.org). A.C.A. was supported by the National Science Foundation Graduate Research Fellowship under Grant No. DGE-1144085. The authors would like to thank Jiahao Kang of the Nanoelectronics Research Lab (http://nrl.ece.ucsb.edu/) at UCSB for lending his expertise in drawing the TOC graphic image.

REFERENCES AND NOTES

1. Bergveld, P. Development of an Ion-Sensitive Solid-State Device for Neurophysiological Measurements. *Biomed. Eng., IEEE Trans.* **1970**, 70–71.
2. Yang, W.; Ratinac, K. R.; Ringer, S. P.; Thordarson, P.; Gooding, J. J.; Braet, F. Carbon Nanomaterials in Biosensors: Should You Use Nanotubes or Graphene? *Angew. Chem., Int. Ed.* **2010**, *49*, 2114–2138.
3. Cui, Y.; Wei, Q.; Park, H.; Lieber, C. M. Nanowire Nanosensors for Highly Sensitive and Selective Detection of Biological and Chemical Species. *Science* **2001**, *293*, 1289–1292.
4. Makowski, M. S.; Ivanisevic, A. Molecular Analysis of Blood with Micro-/Nanoscale Field-Effect-Transistor Biosensors. *Small* **2011**, *7*, 1863–1875.
5. Geim, A. K.; Novoselov, K. S. The Rise of Graphene. *Nat. Mater.* **2007**, *6*, 183–191.
6. Ang, P. K.; Chen, W.; Wee, A. T. S.; Loh, K. P. Solution-Gated Epitaxial Graphene as pH Sensor. *J. Am. Chem. Soc.* **2008**, *130*, 14392–14393.
7. Ohno, Y.; Maehashi, K.; Yamashiro, Y.; Matsumoto, K. Electrolyte-Gated Graphene Field-Effect Transistors for Detecting pH and Protein Adsorption. *Nano Lett.* **2009**, *9*, 3318–3322.
8. Ohno, Y.; Maehashi, K.; Matsumoto, K. Label-Free Biosensors Based on Aptamer-Modified Graphene Field-Effect Transistors. *J. Am. Chem. Soc.* **2010**, *132*, 18012–18013.
9. Dankerl, M.; Hauf, M. V.; Lippert, A.; Hess, L. H.; Birner, S.; Sharp, I. D.; Mahmood, A.; Mallet, P.; Veuillen, J. Y.; Stutzmann, M. Graphene Solution-Gated Field-Effect Transistor Array for Sensing Applications. *Adv. Funct. Mater.* **2010**, *20*, 3117–3124.
10. Radisavljevic, B.; Radenovic, A.; Brivio, J.; Giacometti, V.; Kis, A. Single-Layer MoS_2 Transistors. *Nat. Nanotechnol.* **2011**, *6*, 147–150.
11. Mak, K. F.; Lee, C.; Hone, J.; Shan, J.; Heinz, T. F. Atomically Thin MoS_2: A New Direct-Gap Semiconductor. *Phys. Rev. Lett.* **2010**, *105*, 136805.
12. Brivio, J.; Alexander, D. T.; Kis, A. Ripples and Layers in Ultrathin MoS_2 Membranes. *Nano Lett.* **2011**, *11*, 5148–5153.
13. Bertolazzi, S.; Brivio, J.; Kis, A. Stretching and Breaking of Ultrathin MoS_2. *ACS Nano* **2011**, *5*, 9703–9709.
14. Kim, S.; Konar, A.; Hwang, W.-S.; Lee, J. H.; Lee, J.; Yang, J.; Jung, C.; Kim, H.; Yoo, J.-B.; Choi, J.-Y. High-Mobility and Low-Power Thin-Film Transistors Based on Multilayer MoS_2 Crystals. *Nat. Commun.* **2012**, *3*, 1011.
15. Perera, M. M.; Lin, M.-W.; Chuang, H.-J.; Chamlagain, B. P.; Wang, C.; Tan, X.; Cheng, M. M.-C.; Tománek, D.; Zhou, Z. Improved Carrier Mobility in Few-Layer MoS_2 Field-Effect Transistors with Ionic-Liquid Gating. *ACS Nano* **2013**, *7*, 4449–4458.
16. Lee, G.-H.; Yu, Y.-J.; Cui, X.; Petrone, N.; Lee, C.-H.; Choi, M. S.; Lee, D.-Y.; Lee, C.; Yoo, W. J.; Watanabe, K. Flexible and Transparent MoS_2 Field-Effect Transistors on Hexagonal Boron Nitride-Graphene Heterostructures. *ACS Nano* **2013**, *7*, 7931–7936.
17. Qiu, H.; Pan, L.; Yao, Z.; Li, J.; Shi, Y.; Wang, X. Electrical Characterization of Back-Gated Bi-Layer MoS_2 Field-Effect Transistors and the Effect of Ambient on Their Performances. *Appl. Phys. Lett.* **2012**, *100*, 123104–123104−3.
18. Wu, H.; Yang, R.; Song, B.; Han, Q.; Li, J.; Zhang, Y.; Fang, Y.; Tenne, R.; Wang, C. Biocompatible Inorganic Fullerene-Like Molybdenum Disulfide Nanoparticles Produced by Pulsed Laser Ablation in Water. *ACS Nano* **2011**, *5*, 1276–1281.
19. Novoselov, K.; Jiang, D.; Schedin, F.; Booth, T.; Khotkevich, V.; Morozov, S.; Geim, A. Two-Dimensional Atomic Crystals. *Proc. Natl. Acad. Sci. U.S.A.* **2005**, *102*, 10451–10453.
20. Fang, H.; Chuang, S.; Chang, T. C.; Takei, K.; Takahashi, T.; Javey, A. High-Performance Single Layered WSe_2 P-FETs with Chemically Doped Contacts. *Nano Lett.* **2012**, *12*, 3788–3792.
21. Liu, W.; Kang, J.; Sarkar, D.; Khatami, Y.; Jena, D.; Banerjee, K. Role of Metal Contacts in Designing High-Performance Monolayer n-Type WSe_2 Field Effect Transistors. *Nano Lett.* **2013**, *13*, 1983–1990.
22. Fang, H.; Tosun, M.; Seol, G.; Chang, T. C.; Takei, K.; Guo, J.; Javey, A. Degenerate N-Doping of Few-Layer Transition Metal Dichalcogenides by Potassium. *Nano Lett.* **2013**, *13*, 1991–1995.
23. Lopez-Sanchez, O.; Lembke, D.; Kayci, M.; Radenovic, A.; Kis, A. Ultrasensitive Photodetectors Based on Monolayer MoS_2. *Nat. Nanotechnol.* **2013**, *7*, 497–501.
24. Zhu, C.; Zeng, Z.; Li, H.; Li, F.; Fan, C.; Zhang, H. Single-Layer MoS_2-Based Nanoprobes for Homogeneous Detection of Biomolecules. *J. Am. Chem. Soc.* **2013**, *135*, 5998–6001.
25. He, Q.; Zeng, Z.; Yin, Z.; Li, H.; Wu, S.; Huang, X.; Zhang, H. Fabrication of Flexible MoS_2 Thin-Film Transistor Arrays for Practical Gas-Sensing Applications. *Small* **2012**, *8*, 2994–2999.
26. Li, H.; Yin, Z.; He, Q.; Li, H.; Huang, X.; Lu, G.; Fam, D. W. H.; Tok, A. I. Y.; Zhang, Q.; Zhang, H. Fabrication of Single- and Multilayer MoS_2 Film-Based Field-Effect Transistors for Sensing NO at Room Temperature. *Small* **2012**, *8*, 63–67.
27. Perkins, F.; Friedman, A.; Cobas, E.; Campbell, P.; Jernigan, G.; Jonker, B. Chemical Vapor Sensing with Monolayer MoS_2. *Nano Lett.* **2013**, *13*, 668–673.
28. Late, D. J.; Huang, Y.-K.; Liu, B.; Acharya, J.; Shirodkar, S. N.; Luo, J.; Yan, A.; Charles, D.; Waghmare, U. V.; Dravid, V. P. Sensing Behavior of Atomically Thin-Layered MoS_2 Transistors. *ACS Nano* **2013**, *7*, 4879–4891.
29. Bajwa, S. Z.; Mustafa, G.; Samardzic, R.; Wangchareansak, T.; Lieberzeit, P. A. Nanostructured Materials with Biomimetic Recognition Abilities for Chemical Sensing. *Nanoscale Res. Lett.* **2012**, *7*, 1–7.
30. Wu, S.; Zeng, Z.; He, Q.; Wang, Z.; Wang, S. J.; Du, Y.; Yin, Z.; Sun, X.; Chen, W.; Zhang, H. Electrochemically Reduced Single-Layer MoS_2 Nanosheets: Characterization, Properties, and Sensing Applications. *Small* **2012**, *8*, 2264–2270.
31. The key concepts and results of this work had been highlighted in the Keynote talk: "2D Electronics: Graphene and Beyond" by K. Banerjee on Sept 19, 2013, at the 43rd European Solid-State Device Conference (ESSDERC), Bucharest, Romania, September 16−20, 2013. (http://essderc2013.imt.ro/plenary_talks_Kaustav_Banerjee.shtml).

Slides available at http://nrl.ece.ucsb.edu/sites/default/files/sites/default/papers/ESSDERC-2013-Keynote_KB.pdf.
32. Deen, M. J.; Shinwari, M. W.; Ranuárez, J.; Landheer, D. Noise Considerations in Field-Effect Biosensors. *J. Appl. Phys.* **2006**, *100*, 074703–074703−8.
33. Castellanos-Gomez, A.; Agraït, N.; Rubio-Bollinger, G. Optical Identification of Atomically Thin Dichalcogenide Crystals. *Appl. Phys. Lett.* **2010**, *96*, 213116–213116−3.
34. Coleman, J. N.; Lotya, M.; O'Neill, A.; Bergin, S. D.; King, P. J.; Khan, U.; Young, K.; Gaucher, A.; De, S.; Smith, R. J. Two-Dimensional Nanosheets Produced by Liquid Exfoliation of Layered Materials. *Science* **2011**, *331*, 568–571.
35. Smith, R. J.; King, P. J.; Lotya, M.; Wirtz, C.; Khan, U.; De, S.; O'Neill, A.; Duesberg, G. S.; Grunlan, J. C.; Moriarty, G. Large-Scale Exfoliation of Inorganic Layered Compounds in Aqueous Surfactant Solutions. *Adv. Mater.* **2011**, *23*, 3944–3948.
36. Liu, K.-K.; Zhang, W.; Lee, Y.-H.; Lin, Y.-C.; Chang, M.-T.; Su, C.-Y.; Chang, C.-S.; Li, H.; Shi, Y.; Zhang, H. Growth of Large-Area and Highly Crystalline MoS_2 Thin Layers on Insulating Substrates. *Nano Lett.* **2012**, *12*, 1538–1544.
37. Zhan, Y.; Liu, Z.; Najmaei, S.; Ajayan, P. M.; Lou, J. Large-Area Vapor-Phase Growth and Characterization of MoS_2 Atomic Layers on a SiO_2 Substrate. *Small* **2012**, *8*, 966–971.
38. Wang, H.; Yu, L.; Lee, Y.-H.; Shi, Y.; Hsu, A.; Chin, M. L.; Li, L.-J.; Dubey, M.; Kong, J.; Palacios, T. Integrated Circuits Based on Bilayer MoS_2 Transistors. *Nano Lett.* **2012**, *12*, 4674–4680.
39. Heller, I.; Janssens, A. M.; Männik, J.; Minot, E. D.; Lemay, S. G.; Dekker, C. Identifying the Mechanism of Biosensing with Carbon Nanotube Transistors. *Nano Lett.* **2008**, *8*, 591–595.
40. Kauffman, D. R.; Star, A. Electronically Monitoring Biological Interactions with Carbon Nanotube Field-Effect Transistors. *Chem Soc. Rev.* **2008**, *37*, 1197–1206.
41. Sarkar, D.; Banerjee, K. Proposal for Tunnel-Field-Effect-Transistor as Ultra-Sensitive and Label-Free Biosensors. *Appl. Phys. Lett.* **2012**, *100*, 143108–143108−4.
42. Ortiz-Conde, A.; Garca Sánchez, F.; Liou, J. J.; Cerdeira, A.; Estrada, M.; Yue, Y. A Review of Recent MOSFET Threshold Voltage Extraction Methods. *Microelectron. Reliab.* **2002**, *42*, 583–596.
43. Bergveld, P.; Van Hal, R.; Eijkel, J. The Remarkable Similarity between the Acid-Base Properties of ISFETs and Proteins and the Consequences for the Design of ISFET Biosensors. *Biosens. Bioelectron.* **1995**, *10*, 405–414.
44. Zafar, S.; D'Emic, C.; Afzali, A.; Fletcher, B.; Zhu, Y.; Ning, T. Optimization of pH Sensing Using Silicon Nanowire Field Effect Transistors with HfO_2 as the Sensing Surface. *Nanotechnology* **2011**, *22*, 405501.
45. Gao, X. P.; Zheng, G.; Lieber, C. M. Subthreshold Regime Has the Optimal Sensitivity for Nanowire FET Biosensors. *Nano Lett.* **2009**, *10*, 547–552.
46. Her, R. K. *The Chemistry of Silica*; Wiley: New York, 1979.
47. Taylor, R. F.; Schultz, J. S. *Handbook of Chemical and Biological Sensors*; CRC Press, 2010.
48. Seker, F.; Meeker, K.; Kuech, T. F.; Ellis, A. B. Surface Chemistry of Prototypical Bulk II-VI and III-V Semiconductors and Implications for Chemical Sensing. *Chem. Rev.* **2000**, *100*, 2505–2536.
49. Stern, E.; Klemic, J. F.; Routenberg, D. A.; Wyrembak, P. N.; Turner-Evans, D. B.; Hamilton, A. D.; LaVan, D. A.; Fahmy, T. M.; Reed, M. A. Label-Free Immunodetection with CMOS-Compatible Semiconducting Nanowires. *Nature* **2007**, *445*, 519–522.
50. Stern, E.; Vacic, A.; Rajan, N. K.; Criscione, J. M.; Park, J.; Ilic, B. R.; Mooney, D. J.; Reed, M. A.; Fahmy, T. M. Label-Free Biomarker Detection from Whole Blood. *Nat. Nanotechnol.* **2009**, *5*, 138–142.
51. Schedin, F.; Geim, A.; Morozov, S.; Hill, E.; Blake, P.; Katsnelson, M.; Novoselov, K. Detection of Individual Gas Molecules Adsorbed on Graphene. *Nat. Mater.* **2007**, *6*, 652–655.
52. Guo, X.; Small, J. P.; Klare, J. E.; Wang, Y.; Purewal, M. S.; Tam, I. W.; Hong, B. H.; Caldwell, R.; Huang, L.; O'Brien, S. Covalently Bridging Gaps in Single-Walled Carbon Nanotubes with Conducting Molecules. *Science* **2006**, *311*, 356–359.
53. Goldsmith, B. R.; Coroneus, J. G.; Khalap, V. R.; Kane, A. A.; Weiss, G. A.; Collins, P. G. Conductance-Controlled Point Functionalization of Single-Walled Carbon Nanotubes. *Science* **2007**, *315*, 77–81.
54. Patolsky, F.; Zheng, G.; Hayden, O.; Lakadamyali, M.; Zhuang, X.; Lieber, C. M. Electrical Detection of Single Viruses. *Proc. Natl. Acad. Sci. U.S.A.* **2004**, *101*, 14017–14022.
55. Mohanty, N.; Berry, V. Graphene-Based Single-Bacterium Resolution Biodevice and DNA Transistor: Interfacing Graphene Derivatives with Nanoscale and Microscale Biocomponents. *Nano Lett.* **2008**, *8*, 4469–4476.
56. Datta, S. *Quantum Transport: Atom to Transistor*; Cambridge University Press, 2005.
57. Heller, M. J.; Forster, A. H.; Tu, E. Active Microelectronic Chip Devices Which Utilize Controlled Electrophoretic Fields for Multiplex DNA Hybridization and Other Genomic Applications. *Electrophoresis* **2000**, *21*, 157–164.
58. Graham, D.; Ferreira, H.; Bernardo, J.; Freitas, P.; Cabral, J. Single Magnetic Microsphere Placement and Detection on-Chip Using Current Line Designs with Integrated Spin Valve Sensors: Biotechnological Applications. *J. Appl. Phys.* **2002**, *91*, 7786–7788.
59. Han, M. Y.; Özyilmaz, B.; Zhang, Y.; Kim, P. Energy Band-Gap Engineering of Graphene Nanoribbons. *Phys. Rev. Lett.* **2007**, *98*, 206805.
60. Li, X.; Wang, X.; Zhang, L.; Lee, S.; Dai, H. Chemically Derived, Ultrasmooth Graphene Nanoribbon Semiconductors. *Science* **2008**, *319*, 1229–1232.
61. Jiao, L.; Zhang, L.; Wang, X.; Diankov, G.; Dai, H. Narrow Graphene Nanoribbons from Carbon Nanotubes. *Nature* **2009**, *458*, 877–880.
62. Zhang, Y.; Tang, T.-T.; Girit, C.; Hao, Z.; Martin, M. C.; Zettl, A.; Crommie, M. F.; Shen, Y. R.; Wang, F. Direct Observation of a Widely Tunable Bandgap in Bilayer Graphene. *Nature* **2009**, *459*, 820–823.